J. Fluid Mech. (2011), *vol.* 687, *pp.* 571–583.
doi:10.1017/jfm.2011.394

Quasi-steady linked vortices with chaotic streamlines

Oscar Velasco Fuentes† and Angélica Romero Arteaga

Departamento de Oceanografía Física, CICESE, Ensenada, BC 22860, México

(Received 29 April 2011; revised 24 August 2011; accepted 13 September 2011;
first published online 14 October 2011)

This paper describes the motion and the flow geometry of two or more linked ring vortices in an otherwise quiescent, ideal fluid. The vortices are thin tubes of near-circular shape which lie on the surface of an immaterial torus of small aspect ratio. Since the vortices are assumed to be identical and evenly distributed on any meridional section of the torus, the flow evolution depends only on the number of vortices (n) and the torus aspect ratio (r_1/r_0, where r_0 is the centreline radius and r_1 is the cross-section radius). Numerical simulations based on the Biot–Savart law showed that a small number of vortices ($n = 2, 3$) coiled on a thin torus ($r_1/r_0 \leqslant 0.16$) progressed along and rotated around the symmetry axis of the torus in an almost uniform manner while each vortex approximately preserved its shape. In the comoving frame the velocity field always possesses two stagnation points. The transverse intersection, along $2n$ streamlines, of the stream tube emanating from the front stagnation point and the stream tube ending at the rear stagnation point creates a three-dimensional chaotic tangle. It was found that the volume of the chaotic region increases with increasing torus aspect ratio and decreasing number of vortices.

Key words: chaos, vortex dynamics, vortex interactions

1. Introduction

Ring vortices have been the subject of scientific inquiry for over two hundred years. By the middle of the nineteenth century they had aroused enough interest that Helmholtz (1858) and Rogers (1858) published, with only a few months between them, an analytical study of the motion of *kreisförmige Wirbelfäden* (circular vortex-filaments) and an experimental study of the formation of rotating rings, respectively. A few years later Kelvin (1867) further stimulated the interest in ring vortices with his hypothesis that matter consists of vortex atoms, a misguided conjecture that turned out to be very fruitful in hydrodynamical results. One of the first things Kelvin wondered about was the motion of linked ring vortices. Indeed, on 22 January 1867 he wrote to Helmholtz (Thompson 1910): 'I am, as yet, a good deal puzzled as to what two vortex-rings through one another would do (how each would move, and how its shape would be influenced by the other)'. Kelvin (1875) later deduced, on the basis of conservation of linear and angular vortex impulses, that two linked ring vortices of near-circular shape could be steady solutions of the equations of motion. That is to say, they would

† Email address for correspondence: ovelasco@cicese.mx

rotate uniformly around a fixed line while progressing, also uniformly, along this line. Kelvin did not give the exact shape of the vortices but hypothesized that they should lie on the surface of a torus. In fact, this was only one case of his more general conjecture on the steadiness of individual as well as multiple toroidal filamentary vortices, i.e. thin tubular vortices uniformly coiled on an immaterial torus so that each vortex $V_{p,q}$ winds p times around the symmetry axis of the torus and q times around its centreline before closing on itself. Building on Kelvin's hypothesis, Thomson (1883) analysed the motion of two or more toroidal filamentary vortices. He obtained an approximate analytical expression for the shape of two steady, linked vortices of equal circulation and showed that two linked vortices of unequal circulations could be steady if coiled on two nested tori, whose cross-section radii are specific functions of their circulations. Finally, by considering the limit of infinitely thin vortices lying on the surface of a torus of infinite centreline radius, Thomson (1883) obtained his celebrated result on the stability of a regular polygon of n equal point-vortices.

Almost a century later, Kida (1981) found analytical solutions for individual vortices in the framework of the localized induction approximation (LIA). In this case, the supporting torus generally has an oval cross-section and steady vortices only exist when $q \geqslant p$. Ricca, Samuels & Barenghi (1999) studied the evolution of these vortices under both the Biot–Savart law and the LIA: the numerical simulations based on the Biot–Savart law confirmed the hypotheses of Kelvin (1875), whereas those based on LIA were consistent with the analytical results of Kida (1981). In a sequel study Maggioni *et al.* (2010) analysed the energy and helicity of the vortices and found that writhe contributes more than twist to the overall helicity. Concurrently, Velasco Fuentes (2010) studied the motion and the velocity field of an individual toroidal vortex $V_{p,q}$ as a function of its topology. His analysis, based on the Biot–Savart law and encompassing the parameter region $1 \leqslant p \leqslant 5$ and $1 \leqslant q \leqslant 5$, showed the dominant role of p in determining the speed of the vortex and the geometry of the flow.

In this paper we address the theoretical inferences of Kelvin (1875) and the analytical results of Thomson (1883) by numerically computing the time evolution of linked ring vortices under the Biot–Savart law. Our purpose is twofold: to examine the vortices' uniformity of motion and permanence of form and, once these are reasonably ascertained, to assess the vortices' capacity to carry fluid. In § 2 we discuss the conservation laws discovered by Kelvin, which were the basis for his deductions. The numerical results of § 3 confirm that thin tubular vortices coiled on a torus and linked according to Kelvin's and Thomson's prescriptions are quasi-steady. In § 4 we analyse the velocity field and the transport properties of linked ring vortices. Section 5 contains the conclusions of this work.

2. Integrals of motion

We will assume that the vortices evolve in an inviscid, incompressible, homogeneous fluid which is unbounded and acted on by conservative forces only. Under these circumstances, the kinetic energy, E, and the linear and angular vortex impulses, $\boldsymbol{I}$ and $\boldsymbol{A}$ respectively, are invariants of the motion. When all vorticity is concentrated on line vortices, these conserved quantities are defined as follows:

$$E = \frac{1}{2} \sum_i \Gamma_i \oint \boldsymbol{u} \cdot \boldsymbol{R}_i \times \mathrm{d}\boldsymbol{s}, \tag{2.1}$$

$$\boldsymbol{I} = \frac{1}{2}\sum_i \Gamma_i \oint \boldsymbol{R}_i \times \mathrm{d}\boldsymbol{s} = \sum_i \Gamma_i \int \mathrm{d}\boldsymbol{S}, \tag{2.2}$$

$$\boldsymbol{A} = -\frac{1}{2}\sum_i \Gamma_i \oint R_i^2 \,\mathrm{d}\boldsymbol{s} = \sum_i \Gamma_i \int \boldsymbol{r} \times \mathrm{d}\boldsymbol{S}. \tag{2.3}$$

Here we have used standard notation: the ith vortex, which has circulation Γ_i and moves with velocity $\boldsymbol{u}$, lies on the three-dimensional curve $\boldsymbol{R}_i(s)$; $\mathrm{d}\boldsymbol{s}$ is a line element along this curve; and $\mathrm{d}\boldsymbol{S}$ is the surface element at the point $\boldsymbol{r}$ of an arbitrary surface spanning the closed curve $\boldsymbol{R}_i(s)$. Barenghi, Ricca & Samuels (2001) obtained (2.1) using an expression for the kinetic energy due to Lamb (1879). Kelvin (1875) discovered the conservation of the quantities given by (2.2)–(2.3), but antecedents can be traced back to Maxwell, who stated that 'two ring vortices of any form affect each others area so that the sum of the projection of the two areas on any plane remains constant' (Maxwell & Harman 1995), and to Helmholtz (1858), who showed the conservation of the weighted projected area when the vorticity field is purely azimuthal.

If one or more vortices are coiled on a torus according to Kelvin's (1875) prescription, both $\boldsymbol{I}$ and $\boldsymbol{A}$ are parallel to the axis of the torus. Kelvin thus concluded that toroidal vortices progress along and rotate around the axis of their supporting torus.

3. Vortex evolution

3.1. *Initial conditions and parameter space*

In the initial condition n toroidal ring vortices lie on the surface of an immaterial torus of centreline radius r_0 and cross-section radius r_1. Each vortex is coiled once around the symmetry axis of the torus and once around its centreline, and the set intersects any meridional plane on the vertices of a regular polygon inscribed on the corresponding torus cross-section. All vortices have the same circulation, Γ, and, in a meridional plane, fluid particles rotate in the same sense in the vicinity of each vortex.

Thus the vortices are given, in Cartesian coordinates, as follows:

$$x_i = (r_0 + r_1\cos\phi_i)\cos\theta, \tag{3.1}$$

$$y_i = (r_0 + r_1\cos\phi_i)\sin\theta, \tag{3.2}$$

$$z_i = r_1\sin\phi_i, \tag{3.3}$$

where $i = 1, \ldots, n$ denotes the ith vortex, $\theta \in [0, 2\pi]$ is the angle around the symmetry axis of the torus, and $\phi_i = \theta - 2(n-i)\pi/n$ is the angle around its centreline (see figure 1).

We exclude from our investigation vortices with more complex topology, i.e. $V_{p,q}$ with $p > 1$ or $q > 1$, because a previous study showed that they become more unstable as their complexity increases (Romero Arteaga 2011). For the same reasons we will limit ourselves to the study of small sets of vortices ($n = 2, 3, 4$) coiled on thin tori ($r_1/r_0 < 0.16$). We must further set a lower bound for r_1/r_0 because of the desingularization of the Biot–Savart law, which implies that the vortices have an undeformable cross-section of radius a. Consistency then requires that the vortices are never too close to each other, i.e. their centrelines must be separated by distances about or larger than $3a$. We chose to use a value which amply satisfies this condition for $n = 2$ and narrowly does it for $n = 4$. Therefore in this study the aspect ratio of the torus will be in the range $0.1 < r_1/r_0 < 0.16$ (except for one case in § 4).

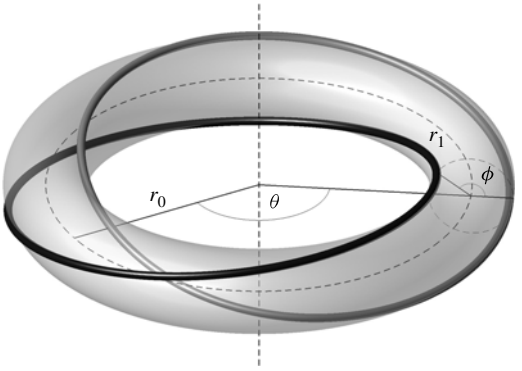

FIGURE 1. Two linked ring vortices represented by light and dark grey tubes. Each vortex is coiled once around the symmetry axis of the torus and once around its centreline. The centreline and cross-section radii of the torus are r_0 and r_1, respectively.

3.2. *Numerical method*

We compute the vortex motion with the Rosenhead–Moore approximation to the Biot–Savart law (see Saffman 1995):

$$\frac{\mathrm{d}\boldsymbol{x}}{\mathrm{d}t} = -\frac{\Gamma}{4\pi}\sum_i \oint \frac{[\boldsymbol{x} - \boldsymbol{R}_i(s)] \times \mathrm{d}\boldsymbol{s}}{(|\boldsymbol{x} - \boldsymbol{R}_i(s)|^2 + \mu^2 a^2)^{3/2}}, \tag{3.4}$$

The use of this approximation implies that the vortices are no longer infinitely thin: they now have an undeformable, circular cross-section of radius a. The value of the radius is chosen to be $a = 0.05$. That of the constant μ depends on the vortex internal structure; the particular value used here, $\mathrm{e}^{-3/4}$, corresponds to uniform vorticity on the vortex cross-section (Saffman 1995). The effect of other choices of a and μ on the vortex motion and flow geometry will be briefly discussed in the final section.

The evolution (3.4) was numerically solved using a fourth-order Runge–Kutta scheme with fixed time step. In order to evaluate the integral on the right-hand side, we represented each vortex with a set of material markers. We chose the number of markers as $m \approx 2L/a$, where L is the vortex length, and the time step as $\mathrm{d}t \approx a^2/\Gamma$, because preliminary tests showed that these values resulted in accurate simulations of the motion of a circular ring, i.e. the shape was preserved and the speed deviated less than 0.5 % from the analytical value. Higher spatial and/or temporal resolutions substantially increased the computational costs without providing major improvements to the accuracy. Since the vortices evolved without significant changes in length or shape it was not necessary to update the spatial discretization (e.g. by removing markers which get too close to each other or introducing new ones where the original ones get excessively separated) as is usually done in highly time-dependent flows (see e.g. Baggaley & Barenghi 2011). As a further control, in all simulations we monitored the evolution of the integrals of motion (2.1)–(2.3): the energy varied by less than 0.1 % of its initial value; the linear and angular impulses varied by less than 0.001 and 0.1 % of their initial magnitudes, respectively, while their directions, which initially coincided with the symmetry axis of the torus, deviated from this direction by angles of $\sim$0.0001 s.

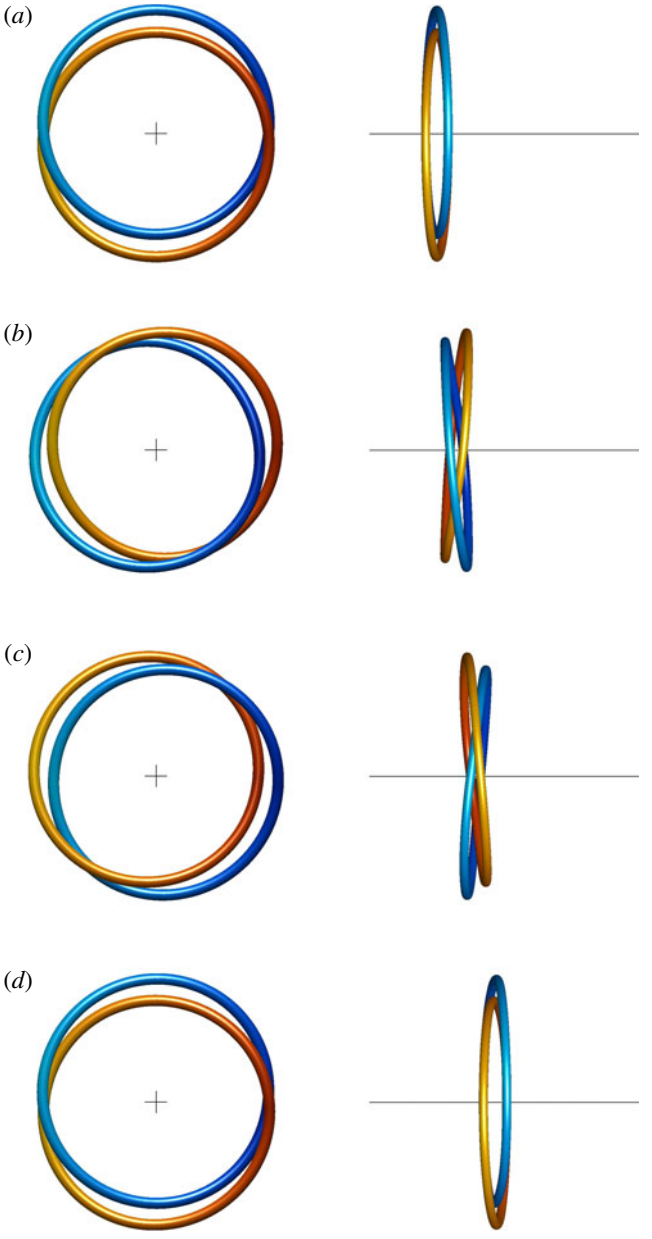

FIGURE 2. Evolution of two linked ring vortices with aspect ratio $r_1/r_0 = 0.1$. The axis of the system is represented by a cross in the frontal view (left column) and by a straight line in the lateral view (right column). The stages depicted are (*a*) $t = 0$, (*b*) $t = 0.105T$, (*c*) $t = 0.210T$, (*d*) $t = 0.315T$, where T is the time required by a circular ring vortex of centreline radius r_0 and cross-section radius a to advance a distance equal to r_0.

3.3. *Progression and rotations of the vortices*

Figure 2 shows an example of the evolution of a pair of linked ring vortices of equal circulation. The vortices (represented by thin, coloured tubes) were initially coiled on a torus of small aspect ratio ($r_1/r_0 = 0.1$). The lateral view shows the progression of

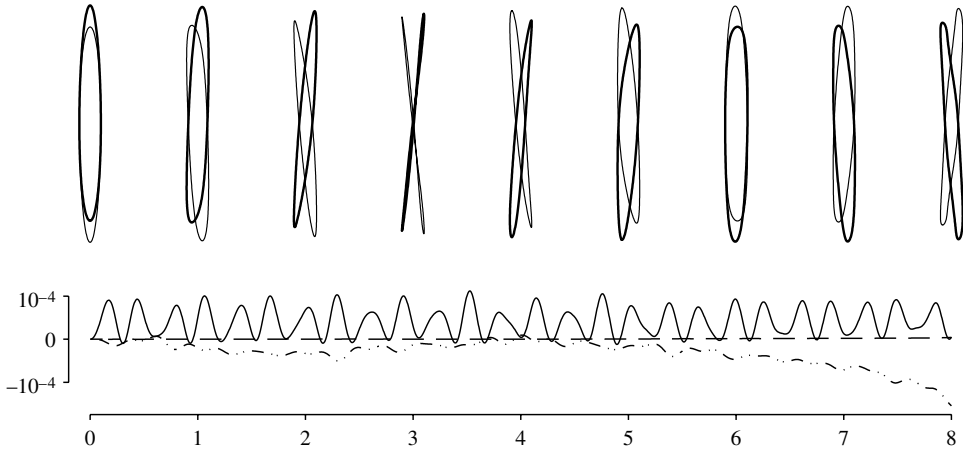

FIGURE 3. (*a*) Progressive motion of a pair of linked vortices (the same of figure 2 but for a 16-times longer period). (*b*) Time evolution of the kinetic energy E (continuous line), linear impulse $\boldsymbol{I}$ (dashed line), and angular impulse $\boldsymbol{A}$ (dot-dashed line). The relative change of these quantities (see text) is shown as a function of the adimensional distance travelled by the vortices, $Z = Ut/r_0$ (where U is the speed of the vortices, t is the time and r_0 is the centreline radius of the torus).

the vortices along the symmetry axis of the torus whereas the front view shows the rotation of the vortices around the same axis. This figure shows exactly one vortex rotation, and since this is relatively fast, the vortices are seen to advance only a short distance during this time.

However, they continue rotating and progressing in the same way for much longer times. Figure 3, for example, shows the vortices advancing a distance equal to eight times their diameter while performing almost sixteen rotations around their symmetry axis. The bottom row of the same figure shows the corresponding time evolution of quantities that, theoretically, should be conserved but which are not exactly so in the numerical simulations. Instead of the instantaneous values of the energy and the linear and angular impulses (2.1)–(2.3), we plotted their relative change; thus figure 3 shows, respectively, $E(t)/E(0) - 1$, $|\boldsymbol{I}(t)|/|\boldsymbol{I}(0)| - 1$ and $|\boldsymbol{A}(t)|/|\boldsymbol{A}(0)| - 1$. In the period shown, the energy is preserved within 0.01 %, the linear impulse within 0.001 %, and the angular impulse within 0.02 %.

The progression of the vortices corresponds, because of Helmholtz's (1858) vortex laws, with the advance of material elements. The vortex rotation around the symmetry axis does not match a similar motion of material elements: it is actually an azimuthal wave. To verify this, note that the hue of the colour in figure 2 marks fluid elements along each vortex and that, in the front view, the darker hues remain on the right-hand side and the lighter ones on the left-hand side of the vortices. The cause of the azimuthal wave is a different motion of the material elements, namely their rotation around the torus centreline. This can be qualitatively verified by close inspection of the vortices' lateral view in figure 2.

Hence the motion of the fluid elements that make up the vortices has two main components: (*a*) progression along the symmetry axis of the torus, and (*b*) rotation around its centreline. We found that these components are approximately uniform so we characterized them by the average speeds U and Ω_c, respectively.

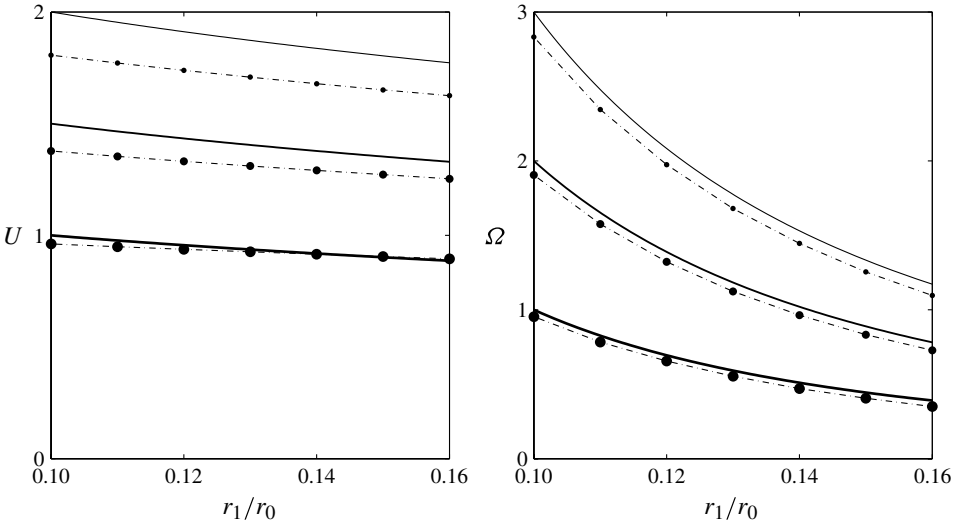

FIGURE 4. Linear speed (U) and phase angular speed (Ω) of the vortex system as functions of the torus aspect ratio (r_1/r_0), for sets of $n = 2$ vortices (thickest line and largest markers), $n = 3$ and $n = 4$ (thinnest line and smallest markers). The continuous lines represent the analytical functions discussed in the text, the markers represent the results of the numerical simulations. The linear speeds are scaled by the speed of a circular ring vortex of circulation 2Γ, centreline radius r_0 and cross-section radius $2a$; the angular speeds are scaled by the rotation speed of a pair of point vortices of circulation Γ separated by a distance $4a$.

The linear speed U grows with the number of vortices n and decreases with the aspect ratio r_1/r_0. A simple argument accounts for this: since $r_1/r_0 \ll 1$ the progression speed behaves as if, instead of n toroidal rings with circulation Γ, there was a single circular ring with cross-section radius r_1 and circulation $n\Gamma$. The speed of this virtual vortex is $U_0 = (n\Gamma/4\pi r_0)[\log(8r_0/r_1) - 1/4]$. Figure 4 shows that this is in good agreement with the speeds measured for sets of linked ring vortices, particularly when $n = 2$.

The angular speed Ω_c increases with n and decreases with r_1/r_0. This can be explained following Thomson (1883): since the vortices are thin and $r_1/r_0 \ll 1$ they move on the meridional plane as if they were a set of point vortices. Indeed, in the parameter region studied here, $\Omega_c \approx 0.94\Omega_0$, where Ω_0 is the angular speed of a set of n point vortices of circulation Γ placed on the vertices of a regular polygon inscribed on a circle of radius r_1: $\Omega_0 = (n-1)\Gamma/4\pi {r_1}^2$. We argued above that the material rotation around the centreline of the torus causes the azimuthal wave around its symmetry axis. The close agreement, shown in figure 4, between Ω_0 and the angular speed of the azimuthal wave, Ω, quantitatively demonstrates the connection between these two rotations.

3.4. *Evolution of the vortex shape*

We applied several diagnostics to measure the deformation of the vortices throughout their evolution. The simplest one was the time evolution of the vortex length, which was observed to vary within 0.3 % of its initial value in the region of the parameter space studied here ($n = 2, 3$ and $0.1 \leqslant r_1/r_0 \leqslant 0.16$). The second diagnostic consisted in finding the torus that best fitted the vortices at every stage of the evolution. The conservation laws (2.2)–(2.3) guarantee that the fitting torus has the same symmetry

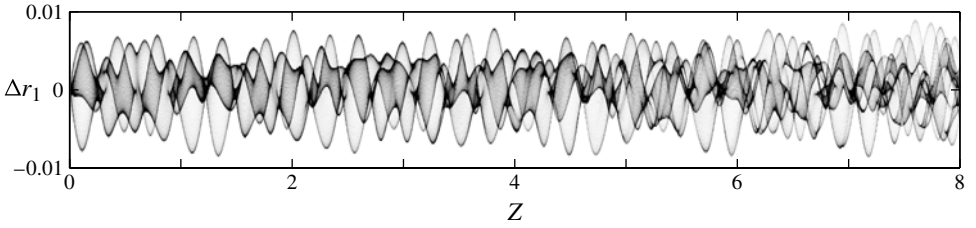

FIGURE 5. Evolution of the vortex shape as illustrated by a time series of the histogram of distances from the vortex markers to the surface of the torus (see text). The signed distance, Δr_1, at which a certain percentage of the markers is located (white, 0 %; black, 100 %) is shown as a function of the adimensional distance travelled by the vortices, $Z = Ut/r_0$ (where U is the speed of the vortices, t is the time and r_0 is the centreline radius of the torus). The results correspond to the simulation shown in figure 3.

axis as the initial one, therefore the former is uniquely determined by the radii $r_0(t)$ and $r_1(t)$. We found that $r_0(t)$ remained within 1 % of its initial value, whereas $r_1(t)$ remained within 5 % of its initial value. The final diagnostic was to measure the signed distance, Δr_1, from the surface of the torus to every material marker representing the vortices. The time series of histograms of Δr_1 showed that the markers remained within a distance $0.01r_0$ of the torus (as in the case $n = 2$, $r_1/r_0 = 0.1$, shown in figure 5).

4. Flow geometry

Toroidal ring vortices are almost stationary and of fixed shape when observed in the comoving frame, i.e. in a coordinate system that translates with speed U and rotates with angular speed Ω. Hence we will use this comoving frame to analyse the flow geometry.

In § 3.3 we showed that the progression speed of a set of n linked vortices with circulation Γ and aspect ratio r_1/r_0 is well approximated by that of a circular ring vortex with circulation $n\Gamma$, centreline radius r_0 and cross-section radius r_1. This implies that, away from the immediate vicinity of the vortices, the velocity field produced by the set of linked vortices may be considered as a small perturbation of the velocity field of a circular ring vortex.

Hence we start by describing the flow geometry of a circular ring vortex in the comoving system (i.e. progressing with speed U). The flow may qualitatively change depending on the numerical value of r_1/r_0, but all values used here fall within the regime of fat ring vortices ($r_1/r_0 > 1/86$: see Saffman 1995 for a detailed analysis). In this regime the velocity field has two stagnation points, both lying on the ring's symmetry axis. The forward one, P, has a linear attractor and a planar repellor; the backward one, Q, has a linear repellor and a planar attractor. The two stagnation points are connected by an infinite number of streamlines starting at P and ending at Q. These lines form a surface with the shape of an oblate spheroid. This stream surface is called a 'separatrix', because the streamlines located inside it are qualitatively different from those located outside it: the former are closed whereas the latter are open and of infinite length. From a more physical point of view, the separatrix is the surface that divides the ambient fluid from the fluid permanently carried by the vortex.

The addition of a solid body rotation, Ω, around the symmetry axis affects neither the existence nor the position of the stagnation points. The rotation transforms the

plane streamlines into helical curves but it leaves the shapes of all stream surfaces unaltered. Therefore, the separatrix of a circular ring vortex in a system progressing with speed U and rotating with speed Ω is the same oblate spheroid described above.

Let us now see what happens when we substitute back the linked vortices in place of the virtual ring vortex. The stagnation points survive, although somewhat displaced. The separatrix, in contrast, disappears: instead of a single surface starting at P and ending at Q, there are now two surfaces. The first one, called the unstable manifold, starts at P and ends infinitely far downstream; the second one, called the stable manifold, starts infinitely far upstream and ends at Q. These surfaces intersect along a finite number of streamlines which start at P and end at Q.

We obtained the unstable manifold by computing a set of streamlines starting on the vicinity of the front stagnation point. The starting points lay on a circle of small radius ($0.01r_0$), coaxial with the torus and centred at the stagnation point. The stable manifold could have been computed in a similar way, but this was unnecessary. Note that a time reversal in the equations of motion is equivalent to a change of sign of all vortex circulations (i.e. $\Gamma \to -\Gamma$) and this is equivalent to the transformation $(x, y, z) \to (x, -y, -z)$, because of the initial conditions described in § 3.1. Therefore, to obtain the stable manifold, we rotated the unstable one by an angle π around the x axis.

Figure 6 shows meridional cross-sections of the stable and unstable manifolds of two linked vortices; each frame corresponds to a supporting torus of a particular aspect ratio ($r_1/r_0 = 0.07, 0.1$). In both cases the thick curve, which represents the unstable manifold of P, smoothly moves downstream but, as it approaches Q, it starts to oscillate about the thin curve, which represents the stable manifold of Q. Similarly, the stable manifold of Q smoothly moves upstream but as it approaches P it starts to oscillate about the unstable manifold of P. Note that when the supporting torus is thinner (figure 6*a*, $r_1/r_0 = 0.07$), the oscillations of the manifolds are of small amplitude and they start close to the opposite stagnation point. In contrast, when the supporting torus is thicker (figure 6*b*, $r_1/r_0 = 0.10$), the oscillations of the manifolds are of larger amplitude and they start closer to their own stagnation point.

The presence of this geometric structure, known as heteroclinic tangle, implies that streamlines are chaotic in this region (see e.g. Wiggins 1992). It also provides a template for the wandering of streamlines around different flow regions through the following mechanism (called 'lobe dynamics': see Rom-Kedar, Leonard & Wiggins 1990 for details). Consider two adjacent intersections, on some meridional plane, between the unstable manifold of P and the stable manifold of Q; the two line segments bounded by these points form a closed contour which defines an area, say A_1, usually called a lobe (see figure 6*b*). The streamlines passing through A_1 successively intersect the same meridional plane within the lobes $A_2, A_3, \ldots$, thus reaching at some point the interior of the so-called vortex atmosphere. This is, however, only a transient situation because the same mechanism eventually brings them out to the downstream side of the vortex.

Figure 6(*b*) shows that there are two independent sequences of lobes, the grey ones and the white ones, which implies that the unstable manifold of P intersects the stable manifold of Q along four streamlines. In fact we found that manifolds always intersect along $2n$ streamlines, where n is the number of vortices. Note also that here, as in all cases we have analysed, the areas of the lobes are larger when they are closer to the symmetry axis of the torus. This occurs because the fluid is incompressible and the azimuthal velocity grows with the distance to the torus axis.

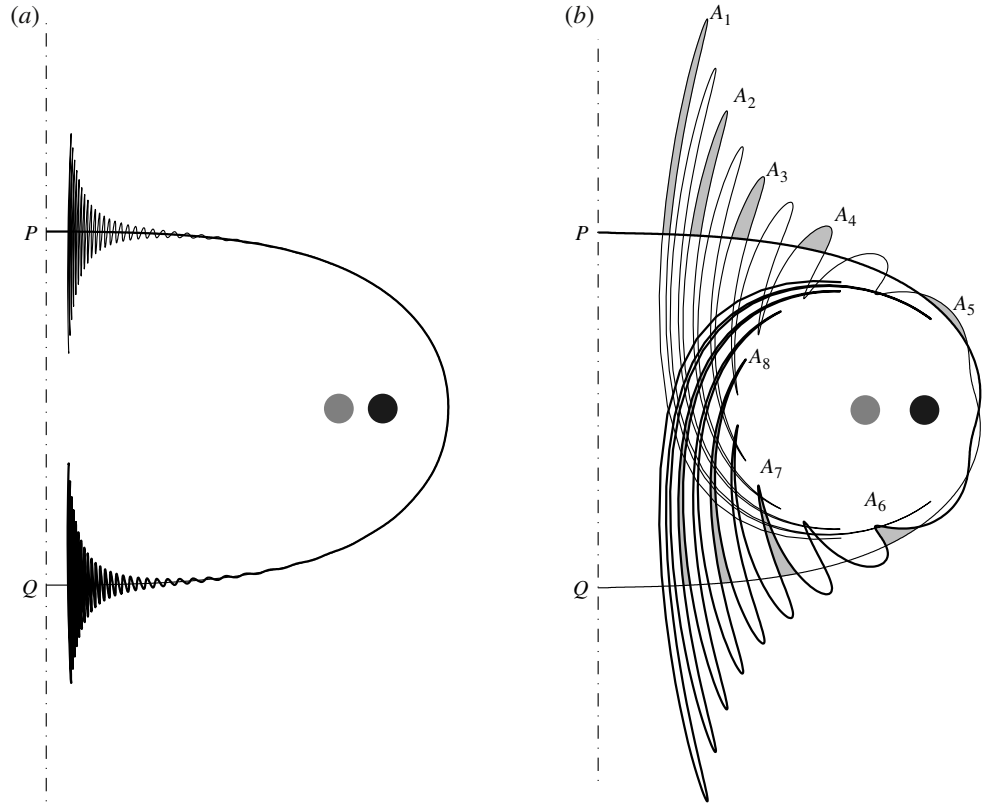

FIGURE 6. Meridional cross-section of the three-dimensional chaotic tangle for n linked ring vortices with aspect ratio r_1/r_0: (a) $n = 2$ and $r_1/r_0 = 0.07$, (b) $n = 2$ and $r_1/r_0 = 0.10$. The thick and thin lines represent, respectively, the unstable manifold of the front stagnation point (P), and the stable manifold of the rear stagnation point (Q); the grey circles represent the vortices and the shaded areas, labelled with A_i, represent successive intersections of a particular streamtube with the meridional plane (see text).

The geometry of the flow around the vortices themselves is best exhibited with the aid of Poincaré sections. We constructed these by numerically computing a set of streamlines that started on a radial line going from the symmetry axis of the torus to the vicinity of the vortices. Then we plotted every intersection of the streamlines with the meridional plane that contains the starting points. Each streamline was colour tagged depending on the position of its starting point: red for those starting closer to the symmetry axis and blue for those starting closer to the vortices (figure 7). We found that the Poincaré section has at least $2n$ large islands of stability: n correspond to the tubes of fluid permanently trapped by an individual vortex, and n correspond to tubes of irrotational fluid which run parallel to the vortices and have approximately the same shape. When $n > 2$ there is an additional island of stability which corresponds to a tube of irrotational fluid that runs between the n vortices and surrounds the torus centreline.

If the number of vortices is large or the aspect ratio of the torus is small, these islands of stability are embedded in a chaotic sea bounded by a nested set of Kolmogorov–Arnold–Moser (KAM) tori, as shown by the bands of differently coloured dots in figure 7(a,c). Note that the largest KAM torus almost fills the

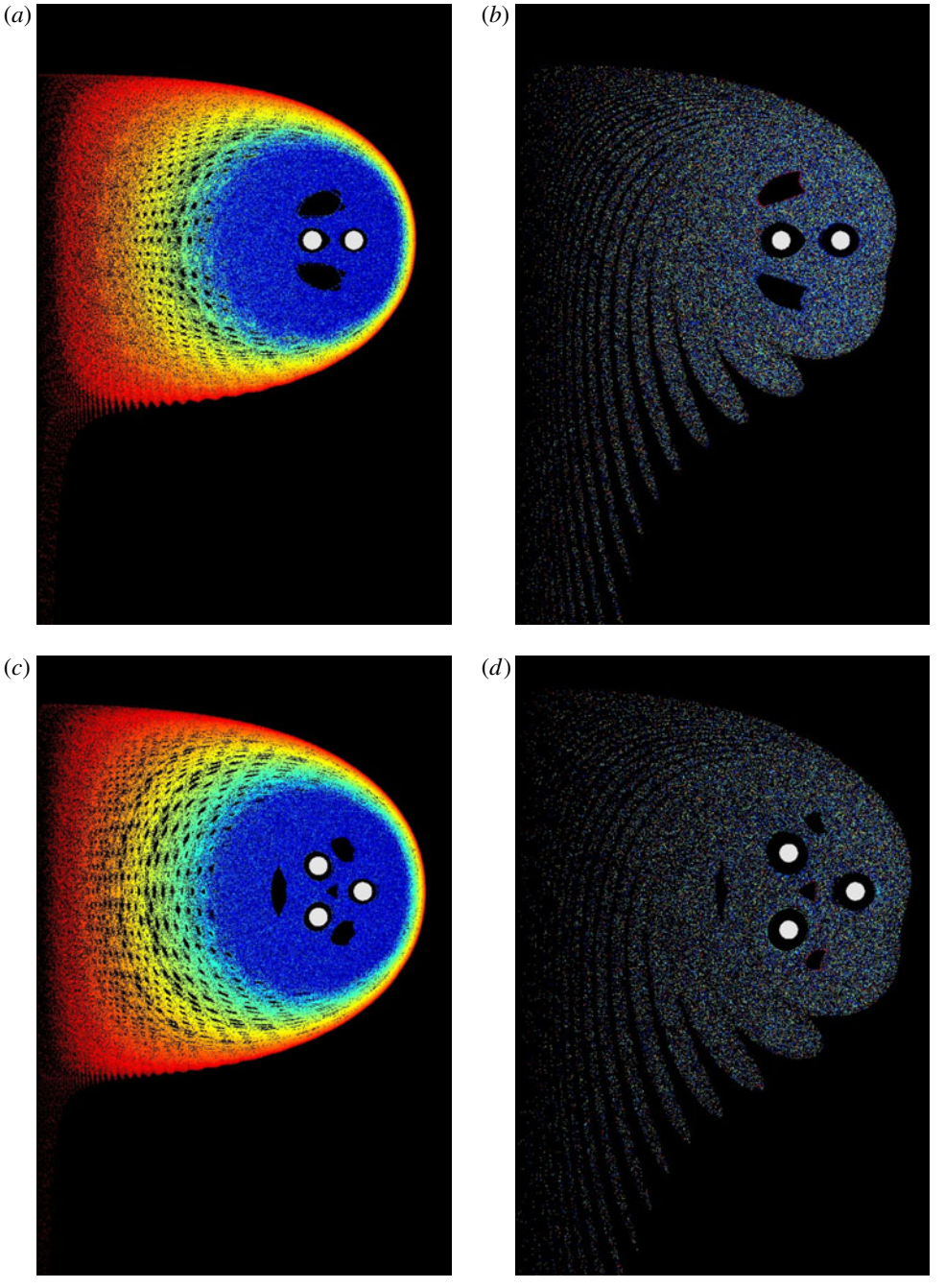

FIGURE 7. Poincaré sections of streamlines in the velocity field of n linked ring vortices with aspect ratio r_1/r_0: (*a*) $n = 2$ and $r_1/r_0 = 0.07$, (*b*) $n = 2$ and $r_1/r_0 = 0.10$, (*c*) $n = 3$ and $r_1/r_0 = 0.10$, (*d*) $n = 3$ and $r_1/r_0 = 0.15$. The intersections of the vortices with the meridional plane $\theta = 0$ are represented by white circles, those of the streamlines by dots coloured according to the position of the streamline's starting point (red, closer to the symmetry axis of the torus; blue, closer to the vortices).

'unperturbed' oblate spheroid. If, however, the number of vortices is small or the aspect ratio of the torus is large, these islands of stability are embedded in an unbounded chaotic sea, as shown by the well-mixed coloured dots in figure 7(*b*,*d*).

5. Discussion and conclusions

Our numerical results confirm Kelvin's (1875) deductions about linked toroidal vortices: they progress along and rotate around the torus symmetry axis with almost uniform speeds while undergoing negligible deformations. The vortices in the approximate solution of Thomson (1883) – a higher-order perturbation, in the small parameter r_1/r_0, of the curves given by (3.1)–(3.3) – behave in the same way. Note that if one uses $\mu = 1$ in (3.4) (Thomson's incorrect value for uniform vortices: see Saffman 1995), the vortex velocity obtained with the numerical model agrees with the analytical result of Thomson (1883), namely $U = (\Gamma/4\pi r_0)[\log(32r_0^2/r_1 a) - 7/4]$.

By proving that both Kelvin's and Thomson's linked vortices move almost uniformly while approximately preserving their shape, we have made plausible the existence of exact solutions which are both steady and stable. Finding the analytical expression of such solutions is, however, still an open problem.

The linked vortices studied here belong to the expanding class of steady or quasi-steady vortices possessing chaotic streamlines, such as vortex knots (Velasco Fuentes 2010) and vortex solitons (Kimura & Koikari 2004). As in these cases, the quasi-steadiness of the linked ring vortices enables us to interpret the results about the flow geometry in terms of the capacity of the vortices to carry fluid. We may thus conclude that more fluid is carried by either more vortices on tori of equal diameter or the same number of vortices on thinner tori. This behaviour is analogous to that of a single toroidal vortex $V_{p,q}$, whose capacity to carry fluid grows as the number of coils round the symmetry axis, p, increases and as the aspect ratio of the torus decreases (see Velasco Fuentes 2010).

Equation (3.4) shows that the velocity field depends on the value of μa, particularly in the neighbourhood of the vortices. This affects the self-induced velocity and, through it, the flow geometry, for if μa is larger the vortices are slower and their stagnation points are closer to each other, and vice versa. To evaluate the extent of the modifications produced by changing the value of μa, we used thinner vortices ($a = 0.025$) with the same internal structure used above ($\mu = \mathrm{e}^{-3/4}$) and hollow vortices ($\mu = \mathrm{e}^{-1/2}$) with the same cross-section used above ($a = 0.05$). The thinner vortices moved with a 6 %-larger speed and the distance between their stagnation points was 8 % smaller. The hollow vortices moved with a 3 %-smaller speed and the distance between their stagnation points was 4 % larger. In neither case did the chaotic tangles or the Poincaré sections exhibit significant changes with respect to those shown in figures 6 and 7.

We are grateful to two anonymous referees for their comments and suggestions on an earlier version of this paper. This research was partially supported by CONACyT (México) through a postgraduate scholarship to ARA.

REFERENCES

BAGGALEY, A. W. & BARENGHI, C. F. 2011 Spectrum of turbulent Kelvin-waves cascade in superfluid helium. *Phys. Rev.* B **83** (13), 134509.

BARENGHI, C. F., RICCA, R. L. & SAMUELS, D. C. 2001 How tangled is a tangle? *Physica* D **157**, 197–206.

HELMHOLTZ, H. 1858 Über Integrale der hydrodynamischen Gleichungen, welche den Wirbelbewegungen entsprechen. *J. Reine Angew. Math.* **55**, 25–55. English translation in *Phil. Mag.* **33** (1867), 485–512.

KIDA, S. 1981 A vortex filament moving without change of form. *J. Fluid Mech.* **112**, 397–409.

KIMURA, Y. & KOIKARI, S. 2004 Particle transport by a vortex soliton. *J. Fluid Mech.* **510**, 201–218.

LAMB, H. 1879 *Treatise on the Mathematical Theory of the Motion of Fluids*. Cambridge University Press.

MAGGIONI, F., ALAMRI, S., BARENGHI, C. F. & RICCA, R. L. 2010 Velocity, energy, and helicity of vortex knots and unknots. *Phys. Rev.* E **82** (2), 026309.

MAXWELL, J. C. & HARMAN, P. M. 1995 *The Scientific Letters and Papers of James Clerk Maxwell: 1862–1873*, vol. 2. Cambridge University Press. Letter to Peter Guthrie Tait, July 1868.

RICCA, R. L., SAMUELS, D. C. & BARENGHI, C. F. 1999 Evolution of vortex knots. *J. Fluid Mech.* **391**, 29–44.

ROGERS, W. B. 1858 On the formation of rotating rings by air and liquids under certain conditions of discharge. *Am. J. Sci. Arts* **26**, 246–258.

ROM-KEDAR, V., LEONARD, A. & WIGGINS, S. 1990 An analytical study of transport, mixing and chaos in an unsteady vortical flow. *J. Fluid Mech.* **214**, 347–394.

ROMERO ARTEAGA, A. 2011 Vórtices eslabonados cuasi-estacionarios. Master's thesis, CICESE.

SAFFMAN, P. G. 1995 *Vortex Dynamics*. Cambridge University Press.

THOMPSON, S. P. 1910 *The Life of William Thomson Baron Kelvin of Largs*, vol. 1. Macmillan.

THOMSON, J. J. 1883 *A Treatise on the Motion of Vortex Rings*. Macmillan.

THOMSON, W. (LORD KELVIN) 1867 On vortex atoms. *Phil. Mag.* **34**, 15–24. Also in *Mathematical and Physical Papers*, vol. 4, pp. 1–12.

THOMSON, W. (LORD KELVIN) 1875 Vortex statics. *Proc. R. Soc. Edin.* **9**, 59–73 Also in *Mathematical and Physical Papers*, vol. 4, pp. 115–128.

VELASCO FUENTES, O. 2010 Chaotic streamlines in the flow of knotted and unknotted vortices. *Theor. Comput. Fluid Dyn.* **24**, 189–193.

WIGGINS, S. 1992 *Chaotic Transport in Dynamical Systems*. Springer.